α-cluster structure and exotic states in a self-consistent model for light nuclei

J. A. Maruhn
Institut für Theoretische Physik, Universität Frankfurt, Max-von-Laue-Str. 1, 60054 Frankfurt am Main, Germany

Masaaki Kimura*
Yukawa Institute for Theoretical Physics, Kyoto 606-8052, Japan

S. Schramm
Institut für Theoretische Physik and Center for Scientific Computing, Universität Frankfurt, Max-von-Laue-Str. 1, 60054 Frankfurt am Main, Germany

P.-G. Reinhard
Institut für Theoretische Physik II, Universität Erlangen-Nürnberg, Staudtstrasse 7, 91058 Erlangen, Germany

H. Horiuchi†
Physics Department, Kyoto University, Kyoto 606-8052, Japan

A. Tohsaki
Suzuki Corporation, 46-22 Kamishima, Kadoma 571-0071, Japan
(Received 27 June 2006; published 26 October 2006)

In this article we examine to what extent traces of α clustering can be found in mean-field ground states of $n\alpha$ nuclei from ^{8}Be through ^{36}Ar as well as in some superdeformed states in ^{32}S, ^{36}Ar, and ^{40}Ca. For this purpose we calculate the overlap of the mean-field Slater determinant with one containing pure Gaussians and perfect spin and isospin symmetry, optimizing the overlap by varying the α-particle positions and radii. In some cases a coherent sum over different configurations is also employed. We find quite large overlaps for some of the lighter systems that diminish for nuclei above ^{20}Ne but again strong clustering in ^{36}Ar.

DOI: 10.1103/PhysRevC.74.044311 PACS number(s): 21.60.Gx, 21.60.Jz, 27.20.+n, 27.30.+t

I. INTRODUCTION

For light $n\alpha$ nuclei, i.e., nuclei composed of $2n$ protons and $2n$ neutrons, a description in terms of α clusters has enjoyed considerable success for many years. In their simplest form, these correspond to mean field with a restricted wave function made up of α clusters: quadruples of particles with both spin and isospin orientations and with Gaussian wave functions in space centered at given positions. These positions are then varied to obtain an optimal many-body wave function. Later variations of this method also allow variation of the radii, allow deformed clusters, and exploit the computational efficiency of the approach to calculate projected states (see [1] and references therein).

In the full Hartree-Fock or mean-field approach, the wave functions can be quite complicated in their spatial behavior and indeed in many modern calculations are freely variable over a coordinate grid, so that typically thousands of values are varied to optimize the many-body wave function. Since the mean-field state is a pure Slater determinant, it does not contain correlations in the conventional sense, which seems to exclude correlated objects like α particles. A closer examination reveals, however, that correlations come in through the mean field. The identical wave functions assumed for each set of four particles in an α-cluster model are present in the full mean-field solution to a certain extent because the eigenfunctions in the same mean-field potential will be filled with four particles, the main cause for deviations from the identical wave functions being spin-orbit coupling (destroying spin degeneracy) and Coulomb effects (destroying isospin degeneracy).

In this article we address the following questions:

(i) To what extent do the mean-field states agree with an $n\alpha$-cluster model; i.e., can they be represented by cluster model wave functions?
(ii) Does this agreement depend in a systematic way on spin orbit strength and the mass of the nuclei?
(iii) Is the mean-field state better represented by a correlated cluster state, in the sense of a coherent sum over different cluster configurations?
(iv) Are there indications for more exotic cluster states producible in the mean-field approach?

It is, of course, interesting to compare the results with cluster model interpretations of these nuclei. In the following discussion, we refer to the geometric configurations suggested by Zhang, Rae, and Merchant [2] based on a cranked version of the Block-Brink α-cluster model. In some cases

*Present address: Institute of Physics, University of Tsukuba, Tsukuba 305-8571, Japan.
†Present address: Research Center for Nuclear Physics, Osaka University, Mihogaoka 10-1, Ibaraki, Osaka 567-0047, Japan.

a comparison to deformed-basis antisymmetrized molecular dynamics (AMD) [3] calculations was also performed.

II. THE MEAN-FIELD CALCULATIONS

A. Method of calculation

We represent the single-particle wave functions on a Cartesian grid with a grid spacing of 1 fm. The grid size is typically 24^3 for ground states and 36×24^2 for superdeformed states. This accuracy was shown to be sufficient to provide converged configurations. The numerical procedure is the damped-gradient iteration method [4], and all derivatives are calculated using the Fourier transform method.

In the case of shape isomeric states, convergence is sometimes difficult to establish. Experience has shown that the observation of the change in total energy alone is not sufficient to judge convergence: this value usually typically decreases rapidly to $\delta E/E \approx 10^{-9}$, which may indicate simply that the calculation is getting stuck and convergence is really stalled. A much better criterion turned out to be the mean-square deviations in the single-particle energies, summed over all states. These uncertainties thus measure how far the states still are from true eigenstates of the single-particle Hamiltonian.

In practice it has often been seen that the total energy seems to converge perfectly well, while the fluctuations in the Hamiltonian stay at a relatively high level of 10^{-3}. In such cases usually the system will stay in this configuration for several thousand iterations and then transit to the ground state relatively rapidly. The underlying situation can be visualized as a steep descent that arrives at some saddle point, where the direction of the descent must be modified strongly, keeping the system at this point for a very large number of iterations. Alternatively it may be caught in a shallow local minimum from which the accumulation of small changes in the wave functions enable the system to escape during further iterations.

B. Interactions and symmetries

We take four different Skyrme forces that all perform very well with regard to nuclear bulk properties but that differ in details: SkM* as a widely used traditional standard [5], Sly6 as a recent fit that includes information on isotopic trends and neutron matter [6], and SkI3 and SkI4 as recent fits that map the relativistic isovector structure of the spin-orbit force [7]. SkI3 contains a fixed isovector part analogous to the relativistic mean-field model, whereas SkI4 is adjusted allowing free variation of the isovector spin-orbit term. Thus all forces differ somewhat in their actual shell structure. Besides the effective mass, the bulk parameters (equilibrium energy and density, incompressibility, symmetry energy) are comparable. In addition we consider two relativistic mean-field models. NL3 is a commonly used parameter set that includes nonlinear interactions of the σ mesons that generate the scalar interaction between the nucleons [8]. The model χ_m is based on a chiral flavor SU(3) effective Lagrangian, which is discussed in detail in [9].

It will be seen that the results are generally in quite good agreement, with mainly the spin-orbit strength producing differences among the Skyrme forces; SkM* systematically deviates somewhat from the others. For NL3 and χ_m the spin-orbit interactions are a direct consequence of the relativistic description of the nucleon wave functions. The treatment of the center-of-mass motion in SkM* is considerably different from that in the other forces; because we do not include a center-of-mass correction, there are considerable differences in the binding energies of light nuclei.

The wave functions were not subject to any symmetry requirements, having neither good spin nor good parity quantum numbers; in fact, the initialization purposely avoided symmetries to make sure that they were not accidentally maintained.

The calculations included pairing in the BCS approximation with a delta force, taking into account three times the number of occupied states without pairing. The parameters were the ones usually associated with each Skyrme force.

C. Observables

The principal observables that will be quoted are the total binding or excitation energy, the spin-orbit energy, the deformation, and the intrinsic quadrupole moment. The quadrupole moment was calculated in the standard way as

$$Q = \int \mathrm{d}^3 r \rho(\vec{r})(3z^2 - r^2) \tag{1}$$

for the case that the z axis is the axis of axial symmetry. A deformation parameter is then obtained as

$$\beta_{20} = \sqrt{\frac{\pi}{5}} \frac{Q}{AR^2}, \tag{2}$$

where A is the mass number and R the mean-square radius of the system. This prescription is, of course, not unique, because the dependence on the mean-square radius is somewhat arbitrary, but follows [10]. Oblate deformations are recognizable by the negative sign in Q_{20} and β_{20}.

III. METHODS OF ANALYSIS

To investigate possible molecular structure, three different methods of analyzing the mean-field Slater determinant $|\Psi\rangle$ were employed. In this section the procedures are described; detailed results for the various nuclei are given in Secs. V and VI.

A. $n\alpha$-cluster model

We investigated the clustering structure by constructing a model many-body wave function with clustering aspects built in and maximizing its overlap with the Slater determinant obtained from the mean-field calculation. As the single-particle wave functions have no good quantum numbers aside from the energy, only the overlap of the complete Slater determinants can be meaningfully investigated. In the case of the relavistic models we used the upper components of the wave functions to calculate the overlap.

In the simplest case, which we refer to as the $n\alpha$-model, the model wave function is constructed completely out of α-particle configurations. For a nucleus with A nucleons,

we use $N_\alpha = A/4$ clusters located at $\vec{r}_k, k = 1, \ldots, N_\alpha$, and with radius parameters σ_k. Depending on the total number of α particles, we usually constrained their radii to be equal, but sometimes, when total computing time allowed, we also allowed them to vary to see whether the overlap was thereby improved. The resulting improvement was of the order of a few percent typically; therefore, in most cases we will quote results only with one common value of σ adjusted for maximum total overlap.

The spatial part of the wave functions then is given by

$$\phi_k(\vec{r}) = A_k \exp\left[-\frac{(\vec{r}-\vec{r}_k)^2}{2\sigma_k^2}\right], \quad k = 1, \ldots, N_\alpha, \qquad (3)$$

with A_k a normalization factor that is computed numerically. The numerical normalization factor calculated on the same spatial grid with 1 fm grid spacing as the mean-field wave functions was found to agree with the analytic one to five significant digits, so that the spatial grid appears sufficiently accurate for the overlap calculations. Each of these wave functions occurs four times in the model Slater determinant: for proton and neutron and with spin up or down.

Note that the $n\alpha$-cluster single-particle wave functions are not orthogonal. As a consequence, the norm of the model Slater determinant must be calculated as the determinant of the single-particle overlaps

$$\mathcal{N} = \det(\langle\phi_j^*|\phi_k\rangle). \qquad (4)$$

This determinant can become very small if the wave functions have large overlaps, which occur frequently in the optimal configurations, indicating that the cluster description does not correspond to clearly separated α particles, but generates the mean-field states largely by antisymmetrization. For example, two Gaussians with the centers placed very close to each other generate an odd-parity state through antisymmetrization.

The overlap $\mathcal{O} = |\langle\Psi|\Phi\rangle|^2$ given in the tables below is always the absolute square of the matrix element between the mean-field Slater determinant and the normalized $n\alpha$-cluster wave function $|\Phi\rangle$; therefore, it describes the probability for the mean-field state to agree with the cluster model state. Because the mean-field wave functions have good isospin but are mixed in spin projection, the total overlap could be simplified by decomposition into a proton and a neutron factor. Although the effects of Coulomb are practically negligible, the calculation did treat the two isospins separately.

B. Calculation of $n\alpha$-cluster configurations

The most effective method to search for the optimal positions and sizes of the $n\alpha$-cluster positions was a search with an optimization algorithm starting from random positions (within a box roughly corresponding to the nuclear volume) and a standard starting value for the radius parameters of 1.8 fm. We found that optimizing the logarithm of the overlap of the two Slater determinants with the algorithm of Stewart [11] (available as routine "dmnfb" in NETLIB) led to very rapid convergence even when the individual particles were placed very badly initially with a starting overlap of $<10^{-15}$ with the mean-field Slater determinant.

The final configurations could in all cases be decomposed into

(i) isolated α particles in a very well-determined position characterizing the cluster geometry, and
(ii) groups of α particles spaced very closely at distances typically < 0.1 fm. These represent cores made up of larger nuclei, usually ^{12}C or ^{16}O. Because the wave functions in these clusters serve mostly to generate higher shell-model states through antisymmetrization, their geometrical layout appears random. It was found that the overlap with the mean-field wave functions changes only by about 2% when the distance between the particles increases from 0.01 to 0.8 fm. It is largest for the smallest distance, but this can cause numerical problems because of the nearly degenerate wave functions.

It should be noted that the positions found usually showed some alignment with the Cartesian axes even for spherically symmetric nuclei, because the representation on a Cartesian grid violates that symmetry to a small but noticeable degree.

In some cases a fixed geometry was also employed to check how different cluster geometries compete in describing the Hartree-Fock (HF) ground state. In these cases a small number of geometric quantities were varied to achieve optimal overlap.

C. Model of core nucleus with additional α particles

In some cases, a model wave function was used where a core of ^{12}C or ^{16}O replaced the corresponding number of α particles. Note that the wave functions used for these were simply static mean-field solutions for those core nuclei, without any adjustable parameters (except for the position of their centers). In the cases where three or four α particles tended to contract into the same location, this may produce more stable numerical results because of the norm going to zero for the α-particle case. The most interesting application of this technique is to the interpretation of the strongly deformed state of ^{32}S as an $^{16}\mathrm{O} + {}^{16}\mathrm{O}$ configuration.

D. Overlap with a collective cluster space

In some cases it was tried to allow some parameter determining the $n\alpha$-cluster configuration to vary in the model wave function and to calculate the overlap with the collective space generated in this way. As an example, in the case of the strongly deformed ^{32}S with Slater determinant state $|\Psi\rangle$ interpreted as an $^{16}\mathrm{O} + {}^{16}\mathrm{O}$ configuration, the Slater determinants $|\Phi_i\rangle$ consisting of the antisymmetrized combination of two ^{16}O nuclei at distances $d_i, i = 1, \ldots, N$, were used as a nonorthogonal basis. The matrix elements of the overlap kernel for this basis are $A_{ij} = \langle\Phi_i|\Phi_j\rangle$. The probability for the state $|\Psi\rangle$ to be within this space is given by

$$\mathcal{O} = \sum_{i,j=1}^{N} (A^{-1})_{ij} \langle\Phi_j|\Psi\rangle\langle\Psi|\Phi_i\rangle. \qquad (5)$$

The result depends on N, but converges rapidly as soon as the collective space is sufficiently spanned. The value of N of

course needs to be chosen carefully. We found that numerically the results remain stable for $N < 20$, but usually $n \approx 5$ is already sufficient for convergence.

The criterion of Eq. (5) to extend the Slater state $|\Psi\rangle$ can be reproduced by a coherent superposition of α-model states

$$|\Psi^{(\text{model})}\rangle = \sum_i |\Phi_i\rangle c_i, \tag{6}$$

with optimized coefficients c_i. This ansatz is the discrete version of the celebrated generator coordinate method (GCM) [12] which had, in fact, one of its early successful applications in the realm of the α-cluster model [13]. Note that the criterion (5) compares somewhat different concepts. The mean-field state $|\Psi\rangle$ is the optimum one can achieve in the space of pure Slater states. The GCM ansatz (6), on the other hand, is restricted to Slater states within the α model but goes beyond Slater space in that it can include substantial correlations in its coherent superposition. Despite, or just because, of this conceptual difference, it is most interesting to investigate the mutual overlap of these two lines of approach in Eq. (5).

IV. GENERAL FEATURES OF THE RESULTS

A general feature of all nuclei considered was that the ground states are axially symmetric as well as reflection symmetric for all the forces considered, although neither the initialization nor the computation enforced these symmetries.

We found in all cases that the converged stationary states showed no pairing, so that calculations *without* pairing might appear sufficient. There is, however, the danger that in iterations using the restricted single-particle space of the occupied wave functions the two fragments may get stuck in a local configuration. It is known that without pairing the deformation energy curve is an envelope of many relatively steep curves corresponding to specific configurations and not all of the narrow minima produced for such a configuration remain minima in the envelope.

In practice it was found that only part of the highly deformed states were still produced in the calculation if pairing was included. Although again in the final result pairing disappeared; we therefore discuss only these ultimately stable configurations.

The freedom allowed by the three-dimensional code was found not to be necessary in these pure mean-field cases, as the stationary states in all cases turned out to be axially symmetric. A comparison with $n\alpha$-cluster model wave functions of course required three-dimensional geometry. A code with axial symmetry and the facility for quadrupole constraints was used in some cases to support the results and check deformation dependence.

V. GROUND STATES OF $n\alpha$ NUCLEI

Next we summarize the properties of the $n\alpha$-nuclei below ^{40}Ca. Density contour plots are shown only for cases with interesting structure and only for SkI3; in these the contour lines are spaced by 0.01 fm^{-3}. The contour lines sometimes appear nonsmooth; this is because the graphics program does not interpolate. The physical wave functions are quite smooth owing to Fourier expansion. In all the tables, we use E_{ls} for the spin-orbit energy, and $\mathcal{O}$ for the overlap with $n\alpha$- or collective cluster configurations.

TABLE I. Binding energies in MeV calculated for the nuclei considered in this article with the four Skyrme force parametrizations used.

	^{4}He	^{8}Be	^{12}C	^{16}O	^{20}Ne
Exp.	28.3	56.5	92.2	127.6	160.6
SkI3	27.8	49.7	89.3	128.9	156.8
SkI4	27.7	49.8	89.3	128.6	157.3
SLy6	27.2	49.0	88.6	127.4	155.9
SkM*	26.8	50.1	93.5	128.0	157.9
NL3	33.9	52.9	91.2	128.7	156.6
χ_m	39.3	53.6	88.9	132.3	161.9
	^{24}Mg	^{28}Si	^{32}S	^{36}Ar	
Exp.	198.3	236.5	271.8	306.7	
SkI3	194.7	233.0	267.1	304.8	
SkI4	196.11	234.9	269.4	305.5	
SLy6	194.4	233.1	268.5	304.0	
SkM*	197.6	237.9	275.1	305.5	
NL3	194.1	231.8	265.6	302.2	
χ_m	197.0	235.0	269.5	308.8	

For some specific nuclei we also mention the overlap between the mean-field wave function and the AMD wave function and also that between AMD and the $n\alpha$-cluster wave function. Here the AMD wave function is obtained using the Gogny D1S force [14]. The use of a different type of force will, of course, reduce the agreement with the mean-field calculations, but a comparison is nevertheless instructive.

A. Binding energies

In Table I the binding energies obtained in all of the ground-state calculations are listed for reference together with the experimental values. All calculations contain a large contribution from the center-of-mass correction, which is calculated in different ways: the Skyrme forces SkI3, SkI4, Sly6 and the χ_m model contain a microscopically calculated correction; NL3 uses the harmonic oscillator approximation; and SkM* contains a correction to the nucleonic mass $m \to m - m/A$.

B. Cluster configuration overview

The optimal cluster configurations obtained are described below in detail. To facilitate visualization, we show an overview of the geometry in Fig. 1. Those cases where there is a trivial configuration as well as those without clear structure preference are omitted.

C. The nucleus ^{4}He

The α particle itself is of course an extreme case for a mean-field description. We summarize its properties in

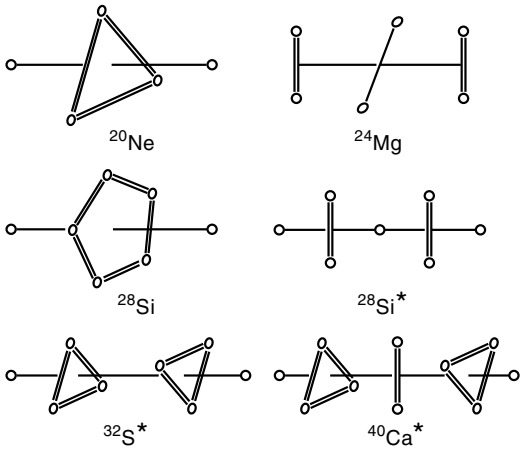

FIG. 1. Visualization of the cluster geometry present in the mean-field ground or excited superdeformed states (denoted by asterisks) for the nontrivial cases. The figures only illustrate the topology; no attempt was made to reproduce correct scale lengths. Double links between particles indicate very small distances. The triangles and pentagon are perpendicular to the linear links.

Table II mostly because it allows us to judge how justified it is to use Gaussian wave functions for the overlap calculations with an $n\alpha$-cluster structure in heavier systems and how the optimum radius depends on the force. For calculating the overlap of the α particle itself with the Gaussian model wave functions, only the radius parameter σ was varied with the optimum value given in the table. In all cases the overlap is remarkably close to one, showing that the use of the Gaussian is a good approximation. Note that in the case of the relativistic descriptions the width of the Gaussian is somewhat smaller than that for the Skyrme forces, which leads to smaller widths throughout the α-cluster analysis presented in this section.

D. The nucleus ^{8}Be

This nucleus is a clear-cut case for a molecular interpretation. For all Skyrme forces considered it turned out to have a necked-in shape agreeing well with a double-α structure interpretation. Density isolines illustrate this in Fig. 2, while other properties are summarized in Table III. The physical properties are quite similar, with SkM* being the odd force out, as expected.

TABLE II. Physical properties of ^{4}He for the different forces considered together with data describing the optimum reproduction by Gaussian wave functions. Note that for the relativistic cases there is no separate *LS*-force, so no E_{ls} values are given.

Force	E_{ls} (MeV)	$R_{\rm rms}$ (fm)	Gaussian model	
			$\mathcal{O}$(%)	σ (fm)
SkI3	0	2.06	99.5	1.67
SkI4	0	2.07	98.8	1.68
Sly6	0	2.12	98.8	1.72
SkM*	0	1.97	99.4	1.61
NL3		1.87	99.4	1.54
χ_m		1.89	89.8	1.54

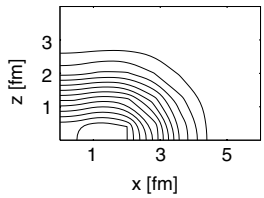

FIG. 2. Density contour lines for ^{8}Be.

The $n\alpha$-cluster analysis naturally found two α particles positioned symmetrically along the symmetry axis with a distance d and a radius of σ. The results in the table indicate that this interpretation works exceedingly well, as even the radius parameters σ agree remarkably well with those for the free α particle. There is, however, a notable nonorthogonality of the two clusters.

This nucleus also gave a good opportunity to test the overlap with α-GCM cluster wave functions as described in Sec. III D. We first used the distance d as a collective coordinate, distributing 10 points in the interval between $d = 1$ fm and $d = 5$ fm and varying σ to maximize the overlap. The result is given in the "α-GCM" column in the tables. The overlap increases noticeably. This calculation was performed only for the Skyrme forces.

It is remarkable that the optimum σ values are smaller for the "α-GCM" case. It may be that for the single-distance analysis the α particles have to widen a bit to simulate the effect of orbital motion; one should not, however, read too much into this as the difference in overlap between the different σ values is of the order of 3%.

The AMD wave function also has a quite large overlap of 96% with the collective two-α-cluster model space. The overlap between the AMD and the mean-field wave function is a little bit smaller at 85%.

E. The nucleus ^{12}C

The surprising feature in this nucleus is the discrepancy in ground-state properties, see Table IV. While three of the Skyrme forces used have a spherical ground state, SkI3 produces a strongly deformed oblate shape. To understand this, a constrained axially symmetric calculation was also performed, which showed that the structure is really quite similar in all cases: the potential is very flat as a function of deformation, and it just happens that the oblate point is about half a MeV lower than the spherical one for SkI3, while this is reversed for the other three forces.

The search for the optimal $n\alpha$-cluster configuration in all cases yielded the α particles very close to the center-of-mass of the nucleus in a roughly triangular configuration. The overlap is much larger for the oblately deformed nucleus, because there is a preferred spatial alignment for the triangle in this case. A calculation with fixed triangular geometry yielded very similar results.

An interpretation with an α-GCM cluster configuration was attempted in two ways. First, a number of different sizes of

TABLE III. Physical properties of ^{8}Be for the four Skyrme forces considered. For the cluster model interpretation the overlap is given together with the optimum distance and radius of the clusters. The last two columns indicate the overlap with an α-GCM model state and the optimal σ obtained.

Force	E_{ls} (MeV)	β_2	Q_{20} (fm^2)	Cluster analysis			α-GCM	
				$\mathcal{O}$(%)	d (fm)	σ (fm)	$\mathcal{O}$(%)	σ (fm)
SkI3	2.5	0.677	46.8	82	2.70	1.68	98	1.65
SkI4	2.7	0.669	46.2	81	2.64	1.69	97	1.64
Sly6	2.4	0.666	48.0	81	2.68	1.73	97	1.68
SkM*	4.6	0.593	38.0	71	2.20	1.68	82	1.62
NL3		0.679	40.7	85	2.52	1.56		
χ_m		0.671	41.8	68	2.60	1.60		

the triangles were used. The configuration that gave converged results was 10 points distributed between 0.01 and 3 fm. This improved the overlap very little, for example, to 30% for SkI3.

Alternatively rotated configurations were included. Adding the Slater determinants for the triangle rotated in its plane by 2–10 equally spaced angles changed the overlap by less than 1%; adding three-dimensional rotations also produced similarly small effects.

The overall disappointingly small overlap with α clusters in this nucleus appears to be due to the large spin-orbit energy, with only the deformed state for SkI3 a better candidate for clustering. This appears to be in contrast to recent FMD [15] as well as older AMD calculations [16,17], which generally show an overlap of about 50% (for later AMD work [18] should be mentioned). To investigate this, we performed calculations with systematically reduced spin-orbit coupling with two of the Skyrme forces. The results, given in Table V, show that the deformation and the cluster overlap are strongly correlated and depend very sensitively on the spin-orbit coupling. Much larger overlaps seem to be possible, but the mean field does not predict the cluster structure very reliably. As the oblate and spherical states are close in energy and not separated by a barrier, including vibrational correlations in the mean-field model will again change the predictions significantly.

A study mixing cluster and shell-model configurations [19] found features qualitatively similar to those of the present work: clustering depends strongly on the spin-orbit force and depending on the interaction the α particles can collapse to a point and approach spin-orbit coupled shell-model configurations in this limit. Since parity and angular momentum were also projected, a quantitative comparison is not useful.

F. The nucleus ^{16}O

For this nucleus all forces produce a spherical ground state, so that in this case the mean-square radius is also an interesting quantity to compare. It is shown in Table VI and it is remarkable that the radii agree very well for all four forces.

The cluster analysis with free placement produced results similar to those of the spherical ^{12}C nuclei: the α particles tended to the same position at the center-of-mass, indicating that one is not dealing with well-separated clusters but again with wave functions produced mainly by antisymmetrization. The optimization located the particles at positions $(d, 0, 0)$, $(0, d, 0)$, $(0, 0, d)$, and $(-d, 0, -d)$, with $d = 0.01$ (as mentioned, results are insensitive to the exact value of d). This is not a natural arrangement, but seems to indicate that the principal requirement is that the four particles not be coplanar. The small variation in the σ values reflects that in the mean-square radii.

A cluster analysis was attempted using a tetrahedron of α particles, with the particles' radii and mutual distance as parameters. The result was that maximizing the overlap

TABLE IV. Physical properties of ^{12}C for the four Skyrme forces considered. The other columns give the maximum overlap with an α-particle configuration for a fixed triangle with side length 0.01 fm.

Force	E_{ls} (MeV)	β_2	Q_{20} (fm^2)	Cluster analysis	
				$\mathcal{O}$(%)	σ
SkI3	15.8	−0.256	−24.7	28	1.72
SkI4	21.6	0.000	0.00	1	1.66
Sly6	19.8	0.000	0.00	1	1.68
SkM*	23.6	0.000	0.00	1	1.64
NL3		0.000	0.00	1	1.48
χ_m		0.129	11.4	2	1.64

TABLE V. Physical properties of ^{12}C for the two Skyrme forces with reduced spin-orbit coupling. The coefficient of the spin orbit strength is multiplied by the factor given, and the consequences for deformation and cluster overlap are shown.

$l * s$ reduction factor	SkI3		Sly6	
	β_2	$\mathcal{O}$(%)	β_2	$\mathcal{O}$(%)
1.0	−0.256	28	0.00	1.68
0.8	−0.326	53	−0.017	1.97
0.6	−0.356	68	−0.303	46
0.4	−0.371	77	−0.337	62
0.2	−0.379	82	−0.356	72
0.0	−0.381	84	−0.367	79

TABLE VI. Properties of ^{16}O for the four Skyrme forces together with results for free cluster placement.

Force	E_{ls} (MeV)	$R_{\rm rms}$ (fm)	Cluster analysis	
			$\mathcal{O}$ (%)	σ (fm)
SkI3	1.0	2.65	96	1.76
SkI4	1.0	2.65	96	1.76
Sly6	0.9	2.69	96	1.79
SkM*	1.1	2.68	96	1.78
NL3		2.56	95	1.72
χ_m		2.58	79	1.71

drives this distance toward zero at $\sigma \approx 1.76$ fm. In this case the limiting overlap is quite close to 1, showing that the tetrahedral symmetry is a good basis for expanding the true wave functions. Like in the case of ^{12}C, however, the cluster interpretation is thus invalid in this case. It should be noted that the overlap, which reaches 98% for a distance of 0.01 fm, only goes down to 97.5% at 0.2 fm. This opens the alternative of either using ^{16}O wave functions or the four-α structure to look for the presence of an ^{16}O core in heavier nuclei.

That the precise arrangement of the clusters is not important was also demonstrated by using fixed geometry. Using an exact tetrahedron configuration produced identical results; only when the particles were coplanar did the overlap vanished immediately.

Our results are in complete agreement with the cluster model of [2].

In view of the good description of this nucleus by static cluster wave functions we did not perform multiconfiguration studies in this case.

G. The nucleus ^{20}Ne

In this case the shape of the nucleus, shown in Fig. 3, shows a strong prolate deformation with a suggestion of a central, more or less spherical part, with two additional mass distributions added on both sides. The physical properties are given in Table VII. This would suggest a ^{12}C core with two α particles added, and this is indeed what was produced by the unconstrained search. This is quite close to the interpretation in [2], although there the central ^{12}C has an annular structure.

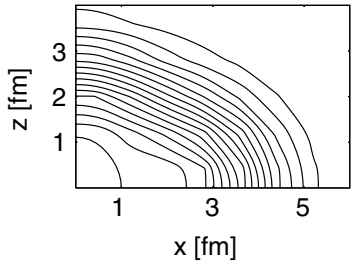

FIG. 3. Density contour lines for ^{20}Ne.

It appeared expedient to try different radii for the α particles in this case. Letting the program optimize all the radii simultaneously instead of using a common σ led to an improvement of <2% in overlap and naturally showed the three particles in the core with the same radius, while the two displaced ones also were identical. The final configuration, for which details are listed in the table, thus has three α particles with radius σ_1 in a triangle at the central position and perpendicular to the longest axis of the nucleus, while two with radius σ_2 are positioned at $\pm d$ along that axis.

An attempt with a multiconfiguration analysis yielded disappointing results: rotating the central triangle gave less than 1% improvement, while allowing the outer particles to move along the axis yielded up to 2%. Adding different sizes of the central triangle gave similar values.

The same 5α configuration is also obtained in an AMD calculation without parity projection before variation. The overlap with the pure $n\alpha$ configuration amounts to 57%. A larger overlap of 61% is obtained by including parity projection before variation. In this case, the optimum configuration corresponds to an $\alpha + ^{16}$O cluster nature. The overlap between the AMD intrinsic wave function obtained without and with parity projection and mean-field wave functions is 78 and 37%, respectively. The intrinsic wave function of AMD in the projected case tends to be parity asymmetric, so that naturally the overlap with the mean-field configuration decreases.

Tomoda and Arima [20] did a very detailed study of an alternative interpretation: an ^{16}O core with an α particle added, which was described by an orbital wave function. This configuration was in turn mixed with a shell-model configuration. For the Skyrme forces we tried a similar configuration by calculating the overlap with a central ^{16}O core and an α particle symmetrized at a distance $\pm d$ from

TABLE VII. Physical properties of ^{20}Ne for the four Skyrme forces considered. The parameters for the cluster analysis are described in the text.

Force	E_{ls} (MeV)	β_2	Q_{20} (fm^2)	Cluster analysis			
				$\mathcal{O}$(%)	d (fm)	σ_1 (fm)	σ_2 (fm)
SkI3	8.5	0.423	91.0	53	1.91	1.78	1.71
SkI4	9.2	0.412	88.0	49	1.86	1.78	1.71
Sly6	8.5	0.409	89.8	47	1.84	1.80	1.74
SkM*	11.1	0.371	79.2	36	1.59	1.77	1.73
NL3		0.425	84.4	59	1.83	1.74	1.65
χ_m		0.439	90.6	50	1.89	1.74	1.69

TABLE VIII. Analysis of ^{20}Ne in terms of an ^{16}O core and a symmetrized α particle at $\pm d$. A GCM variation with the α-particle distance varying is also given.

Force	^{16}O+static α			^{16}O + α GCM	
	$\mathcal{O}$(%)	d (fm)	σ (fm)	$\mathcal{O}$(%)	σ (fm)
SkI3	52	2.7	1.59	54	1.56
SkI4	48	2.5	1.62	49	1.52
Sly6	48	2.6	1.66	49	1.55
SkM*	36	2.4	1.64	36	1.53

the core (symmetrization applied to each single-particle wave function separately). Surprisingly this yielded an even better overlap than the unconstrained pure α configuration, probably because the ^{16}O core contains some of the spin-orbit effects reducing overlap for the pure cluster case. The results, shown in Table VIII, show a somewhat smaller distance between the core and the α particle than the 3.1 fm given in Ref. [20], but are also characterized by smaller radii for the α particle.

We also employed a "GCM" calculation as described in Sec. III D with 10 equidistant values for d between 2 and 4 fm, which produced only small enhancement in the overlap as seen in the table. Varying the number and values of the different d had little effect, but using an unsymmetrized α particle and introducing symmetrization through the GCM distribution reduced the overlap to less than half.

A similar calculation with a ^{12}C core and two α particles on both sides produced results similar to those obtained with the unconstrained pure cluster analysis.

H. The nucleus ^{24}Mg

This nucleus is characterized by a strong quadrupole deformation for all forces considered, as seen in Table IX and Fig. 4.

The unconstrained positioning of the α particles led to a grouping in doublets in the following way: with the x axis being the symmetry axis, two doublets are arranged at $x = \pm p$ with the particles displaced at slightly positive and negative y values (around ± 0.01), while the third doublet is obliquely shifted from the axis to $\pm(0, q, r)$ with p and q surprisingly at larger values. While this appears to show some indications

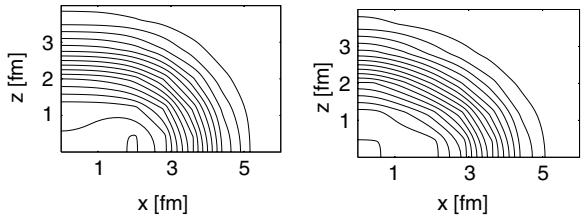

FIG. 4. Density contour lines for ^{24}Mg (left) and ^{28}Si (right).

of true clustering, the overlap is disappointingly small. The oblique positioning of the central doublet again indicates the need for having the spatial degrees of freedom sufficiently represented.

Alternative interpretations with fixed geometrical shape were also explored:

(i) Two equilateral triangles displaced to $x = \pm d$ and either aligned the same way perpendicular to the symmetry axis or rotated by 30° relative to each other. In both cases the maximum overlap that could be achieved by varying the triangle size and d was <0.016. Taking the overlap with two ^{12}C nuclei displaced along the symmetry axis yielded very small overlap ($<10^{-9}$).

(ii) Placing a square with vertices at $x = 0, y, z = \pm q$ and two additional particles at $x = \pm p$ yielded microscopic overlaps of about 0.0002. Clearly this arrangement does not catch the symmetry of the single-particle space near the center.

(iii) Attempts at putting an ^{16}O nucleus into the center, accompanied by two α particles on both sides, lead to much smaller overlap.

The interpretation of Ref. [2] in this case does not agree well; they favor the second of the three choices given. The large value of the spin-orbit energy in our case seems to make a cluster expansion less applicable.

The strong effect of the spin-orbit force to dissolve the cluster structure is also confirmed by the AMD analysis. When the spin-orbit force is switched off, the AMD wave function has a $2\alpha + {}^{16}$O cluster structure and large overlap (56%) with the $n\alpha$-cluster wave function, but a small overlap of a few percent with the mean-field wave function. When the spin-orbit is included, however, the situation turns around: the overlap with the pure $n\alpha$-cluster wave function is reduced to a few percent, whereas that with the mean-field one goes up to 68%.

TABLE IX. Physical properties of ^{24}Mg. The parameters for the cluster analysis are described in the text.

Force	E_{ls} (MeV)	β_2	Q_{20} (fm^2)	Cluster analysis				
				$\mathcal{O}$ (%)	p (fm)	q (fm)	r (fm)	σ (fm)
SkI3	22.6	0.423	117.2	2.3	1.40	0.17	0.37	1.77
SkI4	23.5	0.416	114.1	2.2	1.38	0.10	0.41	1.76
Sly6	21.6	0.413	116.5	2.2	1.39	0.04	0.40	1.79
SkM*	25.4	0.389	107.0	1.8	1.31	0.15	0.41	1.77
NL3		0.416	103.9	2.0	1.37	0.17	0.45	1.71
χ_m		0.431	115.2	2.0	1.38	0.25	0.31	1.74

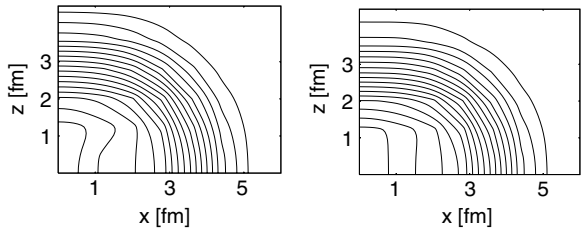

FIG. 5. Density contour lines for ^{32}S and ^{36}Ar.

I. The nucleus ^{28}Si

Except for SkM*, which shows a relatively pure quadrupole deformation, all forces have this nucleus oblate deformed but with a strong hexadecupole contribution visible in the high-density contour lines (see Fig. 4). The oblate deformation is in agreement with other calculations [10,21–23]. Full results are given in Table X.

As suggested by this geometrical shape, the optimal placement resulted in five α particles in a pentagon perpendicular to the symmetry (z) axis and two further particles at symmetric positions on either side. The distances between the particles again tended toward zero, and because of that the pentagon was not a regular polygon. Doing the calculation with a regular pentagon gave identical results for the overlap. The mean-field wave functions thus seem to indicate a preference for the pentagon symmetry, especially in view of the fact that the overlaps are quite large in this case.

J. The nucleus ^{32}S

This nucleus again shows a strong dependence on the force, as seen in Table XI. For SkI3 and SkI4 it is prolate but with the strange feature of an oblate central part at high densities (see Fig. 5), whereas it is spherical for the other two forces. Other self-consistent calculations [10,21–24] generally prefer a prolate deformation. The unconstrained search for an α configuration in this case produced very small overlaps; the geometric positions in all cases appeared almost random, filling a cube near the center-of-mass. The distances, however, in this case were up to the order of 0.5 fm, showing that the overlap is quite insensitive to the particle placement. The very small overlap may be due to the $1s_{1/2}$ filling and the large contribution of the spin-orbit force.

TABLE X. Physical properties of ^{28}Si and optimum cluster parameters.

Force	E_{ls} (MeV)	β_2	Q_{20} (fm^2)	Cluster analysis	
				$\mathcal{O}$(%)	σ (fm)
SkI3	30.2	−0.318	−108.5	7.8	1.86
SkI4	33.6	−0.294	−98.6	4.5	1.85
Sly6	31.7	−0.289	−98.8	4.0	1.87
SkM*	40.6	−0.224	−73.7	0.8	1.83
NL3		−0.303	−93.5	6.2	1.80
χ_m		−0.351	−117.9	14.9	1.85

TABLE XI. Physical properties of ^{32}S for the four Skyrme forces considered.

Force	E_{ls} (MeV)	β_2	Q_{20} (fm^2)	Cluster analysis	
				$\mathcal{O}$(%)	σ
SkI3	29.6	0.222	90.6	1.6	1.87
SkI4	37.0	0.147	58.7	0.3	1.86
Sly6	40.0	0.000	0.0	0.04	1.87
SkM*	44.7	0.000	0.0	0.03	1.86
NL3		0.228	86.24	1.8	1.83
χ_m		0.253	101.1	2.2	1.85

The AMD wave function in this case is closer to the mean-field one with an overlap of 40%, but has only a few percent overlap with the $n\alpha$-cluster wave function.

K. The nucleus ^{36}Ar

This nucleus (results in Table XII) appears as just the opposite of ^{32}S: it is oblate with a deformation in agreement with other calculations [10,21–23], but shows an inner core of prolate deformation at high density. The geometry of the $n\alpha$-cluster configurations found appeared as random as in the case of ^{32}S, but the distances to the center-of-mass were again of the order of <0.1 fm, which together with the much larger overlaps shows that is again a case of a dominating antisymmetrization effect. This comes close to the almost spherical geometry preferred by [2].

It is, of course, somewhat unexpected that in this nucleus clustering appears stronger than for all the others heavier than ^{20}Ne. This should be due to the much reduced role of the spin-orbit coupling in this nucleus as witnessed by the spin-orbit energy being only half of that for ^{32}S.

VI. STRONGLY DEFORMED STATES

A. Technique for searching such states

The search for strongly deformed isomeric states in the mean-field approximation has usually been done with constraints. We tried a new method that has the potential for producing more exotic configurations: initialization of the mean-field calculation with a fragment configuration. Thus, e.g., one may place two ^{16}O nuclei at a certain distance d

TABLE XII. Physical properties of ^{36}Ar and cluster analysis.

Force	E_{ls} (MeV)	β_2	Q_{20} (fm^2)	Cluster analysis	
				$\mathcal{O}$ (%)	σ
SkI3	13.5	−0.183	−90.3	28	1.92
SkI4	15.2	−0.171	−83.8	21	1.91
Sly6	15.1	−0.162	−81.0	17	1.93
SkM*	19.1	−0.133	−65.9	7	1.92
NL3		−0.186	−87.3	33	1.90
χ_m		−0.194	−94.1	29	1.89

from each other into a numerical grid, orthogonalize, and then iterate to converge to a stationary state. For small distances it may converge into the ground state (although we find this rarely happens, because the antisymmetrization produces quite a different set of single-particle orbitals than that of the ground state); for a large d the nuclei may be driven apart; and, finally, for some range convergence may happen in a highly deformed configuration.

The attractive feature of this method is that initial configurations are highly flexible and might lead to configurations that cannot easily be reached with a constraint. For example, a chain or a triangle of three α particles may be used to look for a strongly deformed exotic state in ^{12}C, or one might try various asymmetric mass configurations to investigate whether they all converge to the same deformed state.

With pairing omitted, we found a large number of exotic states, which, however, corresponded to local minima under the constraint of a fixed single-particle configuration. Such minima may be important for the dynamics, as they correspond to a large collective mass when the collective motion in the deformation is slow enough to crossover to another single-particle configuration, but clearly are not isomeric states. We therefore used pairing in the iterations, which made most of the minima disappear; the final states, however, as for the ground states, did not show significant pairing.

B. General features of superdeformed states

A large number of different combinations of $n\alpha$ nuclei leading to compound systems up to ^{40}Ca were considered and the static calculations with different initial fragment positions were performed. Before going into the detailed results given in Table XIII and the following sections, let us summarize the main points of the findings:

(i) Superdeformed shapes were found in the majority of cases, but none of these appears to be of clearly molecular type.
(ii) These exotic states were always axially and reflection symmetric, even if the calculation was started with two nuclei of different mass.
(iii) For the superdeformed states only Skyrme forces SkI3 and Sly6 were employed. Generally the two Skyrme forces yielded similar results, with the excitation energy somewhat more force-dependent than the deformation. We only present results for SkI3 and mention discrepancies to Sly6 where they appear interesting.
(iv) For these cases a comparison to the results of Ref. [2] is not given: although the densities are roughly similar at least in the case of ^{32}S, they did not use a spin-orbit force, which makes the comparison of the cluster interpretations problematic.

The results are summarized in Table XIII.

C. The compound system ^{24}Mg

In the combination of two ^{12}C nuclei, no indication of a superdeformed state was found. The iterations always led either to the ground state of ^{24}Mg or to further separation.

TABLE XIII. Physical properties of highly deformed states for the Skyrme force SkI3 and the chiral model χ_m.

System	E^* (MeV)	E_{ls} (MeV)	β_2	Q_2 (fm^2)	Cluster analysis	
					$\mathcal{O}$ (%)	σ (fm)
			SkI3			
^{28}Si	13.2	25.6	0.773	325.9	1.3	1.80
^{32}S	8.9	12.3	0.737	377.4	34.5	1.79
^{36}Ar	8.7	29.1	0.529	283.4	3	1.88
^{40}Ca	26.3	28.1	0.983	859.8	0.8	1.80
			χ_m			
^{28}Si	11.1		0.775	314.4	1.2	1.77
^{32}S	5.7		0.743	368.6	36.2	1.75
^{36}Ar	9.2		0.533	278.9	1.2	1.84
^{40}Ca	23.7		0.982	829.41	0.8	1.77

D. The compound system ^{28}Si

This is formed in the combination ^{12}C+^{16}O. The iterations led – aside from the ground state of ^{28}Si – to one superdeformed state. Its properties, like those of all the states found, are summarized in Table XIII. The density contour lines show a bit of a double-humped structure at high density (see Fig. 6). The unconstrained cluster analysis showed that along the symmetry axis the particles are grouped in the following way: one is located at a central x position but with a half-fermi displacement in the y and $-z$ directions (this displacement is probably accidental and not significant for the overlap, because it violates overall reflection symmetry). At $\pm$1.23 fm there are pairs of particles on both sides of the axis at a relative distance of about 0.1 fm, while finally two particles are located at $\pm$3.1 fm on the axis. The overlap with the $n\alpha$-cluster configuration is, however, quite small.

E. The compound system ^{32}S

This was studied in two different configurations: ^{12}C+^{20}Ne and ^{16}O+^{16}O, so that an interesting aspect is whether the initial asymmetry is lost. It was found that both configurations converge rapidly into the same state, which is shown in Fig. 6. A state of similar deformation and excitation energy is well known in the literature with similar properties [25–31]. It shows a slight amount of necking-in, making this the best candidate for a "molecular" configuration.

The relatively small spin-orbit energy, compared to that of the other superdeformed states, makes a cluster analysis much more attractive. The unconstrained α analysis shows all

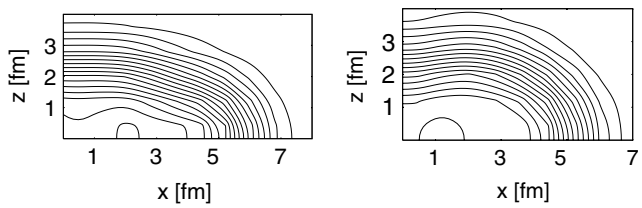

FIG. 6. Density contour lines for ^{28}Si and ^{32}S superdeformed states.

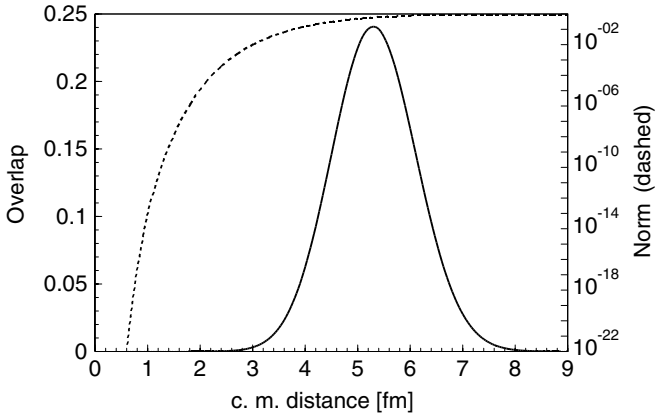

FIG. 7. (Full curve) Overlap of the strongly deformed state found in ^{32}S with a configuration of two ^{16}O nuclei placed symmetrically at a given distance. (Dashed curve) Norm of the combined Slater determinant of the two ^{16}O nuclei.

particles very close (the usual 0.01 fm) to the symmetry axis with two triplets at ±1.9 fm and additional single particles at ±2.82 fm. The center-of-mass of the four particles on each side is at ±2.1 fm. This is a clear indication of a molecular structure with somewhat distorted ^{16}O nuclei at a distance of about 4 fm.

For this reason an analysis of this system based on a double-^{16}O configuration was also attempted. Two ground-state configurations were inserted into the grid at a specified distance, with the two nuclei being displaced symmetrically from the center-of-mass of the compound system along the axis of symmetry. The resulting overlap is shown in Fig. 7 together with the norm of the combined Slater determinant. The resulting maximum overlap indicates that this molecular configuration is not a perfect match; it is only near 6% and, moreover, falls off relatively slowly as the distance is varied. On the other hand, the norm of the model wave function (after orthogonalization) is already close to unity, indicating the possibility of molecular structure at this distance, and using undistorted ^{16}O nuclei for the overlap analysis is a strong constraint.

The small overlap, however, is not the full story. Doing an analysis along the lines of Sec. III D with 20 different c.m. distances used between 3 and 8 fm, we find a total overlap with this collective space of 35%, which agrees surprisingly well with the unconstrained α-particle analysis. The much more comprehensive analysis of this system done by Kimura and Horiuchi [30] gives a somewhat larger overlap of 57%, but is based on a very different wave function and technique, i.e., a comparison of deformed-basis AMD [3] with generator coordinate method to a resonating-group wave function for the double-^{16}O system. It is not surprising that a mean-field description of this strongly deformed state contains less of an $n\alpha$-cluster configuration than the AMD description. The AMD wave function, on the other hand, was found to have a larger overlap with the mean-field one; also its spin-orbit energy is in surprisingly good agreement with the mean-field one. This could be an interesting point for future studies.

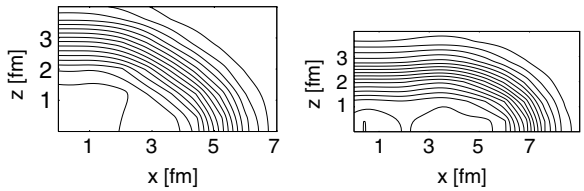

FIG. 8. Density contour lines for ^{36}Ar (left) and ^{40}Ca (right) superdeformed states.

A similar attempt to increase the overlap with the $n\alpha$-cluster configuration by varying the distance between the two quadruplet positions brought no further improvement.

F. The compound system ^{36}Ar

This is somewhat similar in showing a slight necking-in effect, and again the iterations proceeding from the two different initial configurations ^{16}O+^{20}Ne and ^{12}C+^{24}Mg led to the same final state. The shape is shown in Fig. 8. It is interesting that for this system the calculation with pairing found this superdeformed state rapidly from a wide range of initial distances, whereas the unpaired calculation tended to get stuck near $\beta = 1$ and only relaxed to the correct state after several thousand iterations.

The unconstrained α-cluster analysis showed a diffuse picture. The configuration yielding the overlap quoted had two particles at ±2.7 fm, a quadruplet in a distorted rectangle at −0.3 fm, and a triplet at +0.4 fm. The overlap depends only weakly on the precise positioning; this is also consistent, e.g., with the central seven particles placed in two triangles facing each other and a single α between at the center-of-mass.

G. The compound system ^{40}Ca

This is really hyperdeformed as seen in Fig. 8. The density shows a triple-humped structure, which is also borne out by the unconstrained placement of α particles. It produced a configuration characterized by two particles near ±4.3 fm, two particles at the center-of-mass, and two triangular triplets near ±2.9 fm along the symmetry axis. The overlap was quite small, however, and seemed to depend only weakly on the exact placement of the particles, so that the individual particles were up to half a fermi from symmetric positions along the axis. The lateral displacement was always $\leqslant$0.2 fm, though. A further indication that at this point the cluster interpretation becomes quite fuzzy is that for Sly6, which showed a practically identical density distribution, one of the α's from the triangles move closer to those on the end positions.

VII. EXOTIC α-PARTICLE STRUCTURES

It should be briefly mentioned that the present code also allows the search for more exotic α-clustering structures, such as chains and polygons, by initializing the static mean-field calculation with such a geometric arrangement. No interesting

state was found for three- and four-α particles, however, and as an example we confirmed the results of Itagaki and collaborators [32] that a three-α linear chain is unstable with respect to triaxial deformations also for the mean field.

VIII. SUMMARY

The results obtained in this article give a large amount of information on the relationship between cluster wave functions and ground-state mean-field ones. Let us summarize the main features of the ground-state analysis first:

(i) The automatic search for $n\alpha$-cluster configurations with maximal overlap to the mean-field state worked surprisingly well and appears to really produce the best configurations, as all analyses with specific geometric assumptions showed. The geometry of the clusters appears similar to what is produced in cluster calculations.

(ii) Even when it was freely varied, the radius parameter for the α's always had reasonable values. It slowly increased with the mass of the nucleus, indicating the diminishing localization of the particles.

(iii) In all cases, the overlap decreased as the spin-orbit energy produced by a certain force parametrization increased. As expected the spin-orbit coupling destroyed the spin-symmetric cluster structures.

(iv) The overlap with clusters also decreased when going to heavier systems. The growing effects of spin-orbit coupling and Coulomb explain that naturally.

(v) Also as expected the cluster wave functions worked better for the lighter systems up to ^{20}Ne. There was, however, again enhanced overlap for ^{28}Si and ^{36}Ar. It is interesting that the AMD model deviates from a pure $n\alpha$-structure in the same way and stays closer to the mean-field model.

(vi) In many cases the optimal $n\alpha$-structure contains groups of α particles spaced very close together. They do not represent a true α-cluster configuration, but correspond to heavier clusters.

(vii) The attempts at including correlations in the form of collective superpositions were disappointing, producing only minor improvements in the overlaps. Apparently their relatively large size compared to the total nucleus enables the clusters to fill the nucleus without additional spreading.

(viii) The relativistic model results were generally very similar to the Skyrme force ones. The only remarkable difference is in the cluster radii, which were systematically smaller for the relativistic version.

For the superdeformed states the clearest example of cluster structure is ^{32}S, and it is especially interesting that the overlap with the double-^{16}O system agrees very well with that of the unconstrained α configuration.

ACKNOWLEDGMENTS

This work was supported by BMBF under Contracts 06 F 131 and 06 ER 124. We gratefully acknowledge support by the Frankfurt Center for Scientific Computing. One of the authors (J.M.) is indebted to the Japanese Society for the Promotion of Science (JSPS) for support during a visit to Kyoto University, where this research was initiated.

[1] K. Ikeda, H. Horiuchi, S. Saito, Y. Fujiwara, M. Kamimura, K. Katō, Y. Suzuki, E. Uegaki, H. Furutani, H. Kanada, T. Kaneko, S. Nagata, H. Nishioka, S. Okabe, T. Sakuda, M. Seya. Y. Abe, Y. Kondō, T. Matsuse, A. Tohsaki-Suzuki, Y. Fujiwara, H. Horiuchi, K. Ikeda, M. Kamimura, K. Kato, Y. Suzuki, and E. Uegaki, Prog. Theor. Phys. Suppl. **68**, 29 (1980).
[2] J. Zhang, W. D. M. Rae, and A. C. Merchant, Nucl. Phys. **A575**, 61 (1994).
[3] M. Kimura, Phys. Rev. C **69**, 044319 (2004).
[4] P.-G. Reinhard and R. Y. Cusson, Nucl. Phys. **A378**, 418 (1982).
[5] J. Bartel, P. Quentin, M. Brack, C. Guet, and H.-B. Hakansson, Nucl. Phys. **A386**, 79 (1982).
[6] E. Chabanat, P. Bonche, P. Haensel, J. Meyer, and R. Schaeffer, Nucl. Phys. **A627**, 710 (1997).
[7] P.-G. Reinhard and H. Flocard, Nucl. Phys. **A584**, 467 (1995).
[8] G. A. Lalazissis, J. König, and P. Ring, Phys. Rev. C **55**, 540 (1997).
[9] S. Schramm, Phys. Rev. C **66**, 064310 (2002).
[10] T. R. Werner, J. A. Sheikh, M. Misu, W. Nazarewicz, J. Rikovska, K. Heeger, A. S. Umar, and M. R. Strayer, Nucl. Phys. **A579**, 327 (1996).
[11] G. W. Stewart III, J. Assoc. Comput. Mach. **14**, 72 (1967).
[12] J. A. Wheeler and J. J. Griffin, Phys. Rev. **108**, 311 (1957).
[13] D. M. Brink and A. Weiguny, Nucl. Phys. **A120**, 59 (1968).
[14] J. Dechargé and D. Gogny, Phys. Rev. C **21**, 1568 (1980).
[15] T. Neff and H. Feldmeier, Nucl. Phys. **A738**, 357 (2004).
[16] Y. Kanada-En'yo, Phys. Rev. Lett. **81**, 5291 (1998).
[17] N. Itagaki, S. Aoyama, S. Okabe, and K. Ikeda, Phys. Rev. C **70**, 054307 (2004).
[18] Y. Kanada-En'yo, preprint nucl-th/0605047 (2006).
[19] N. Takigawa and A. Arima, Nucl. Phys. **A168**, 593 (1971).
[20] T. Tomoda and A. Arima, Nucl. Phys. **A303**, 217 (1978).
[21] H. R. Jaqaman and L. Zamick, Phys. Rev. C **30**, 1719 (1984).
[22] J. Fink, V. Blim, P.-G. Reinhard, J. Maruhn, and W. Greiner, Phys. Lett. **B218**, 277 (1989).
[23] S. K. Patra and C. R. Praharaj, Nucl. Phys. **A565**, 442 (1993).
[24] M. Girod and B. Grammaticos, Phys. Rev. C **27**, 2317 (1983).
[25] H. Flocard, P. H. Heenen, S. J. Krieger, and M. Weiss, Prog. Theor. Phys. **72**, 1000 (1984).
[26] H. Molique, J. Dobaczewski, and J. Dudek, Phys. Rev. C **61**, 044304 (2000).
[27] M. Yamagami and K. Matsuyanagi, Nucl. Phys. **A672**, 123 (2000).
[28] R. R. Rodríguez-Guzmán, J. L. Egido, and L. M. Robledo, Phys. Rev. C **62**, 054308 (2000).
[29] M. Yamagami and K. Matsuyanagi, Nucl. Phys. **A672**, 123 (2000).
[30] M. Kimura and H. Horiuchi, Phys. Rev. C **69**, 051304(R) (2004).
[31] T. Inakura, S. Mizutori, M. Yamagami, and K. Matsuyanagi, Nucl. Phys. **A728**, 52 (2003).
[32] N. Itagaki, S. Okabe, K. Ikeda, and I. Tanihata, Phys. Rev. C **64**, 014301 (2001).